SuperWASP-North extrasolar planet candidates between 3h <RA <6h

Mon. Not. R. Astron. Soc. **381,** 851–864 (2007) doi:10.1111/j.1365-2966.2007.12294.x

SuperWASP-North extrasolar planet candidates between $3^h < RA < 6^h$

W. I. Clarkson,[1,2⋆] B. Enoch,[1] C. A. Haswell,[1] A. J. Norton,[1] D. J. Christian,[3] A. Collier Cameron,[4] S. R. Kane,[4,5] K. D. Horne,[4] T. A. Lister,[4,6,7] R. A. Street,[3,8] R. G. West,[9] D. M. Wilson,[6] N. Evans,[6] A. Fitzsimmons,[3] C. Hellier,[6] S. T. Hodgkin,[10] J. Irwin,[10] F. P. Keenan,[3] J. P. Osborne,[9] N. R. Parley,[1] D. L. Pollacco,[3] R. Ryans,[3] I. Skillen[11] and P. J. Wheatley[12]

[1]*Department of Physics & Astronomy, The Open University, Milton Keynes MK7 6AA*
[2]*Space Telescope Science Institute, 3700 San Martin Drive, Baltimore, MD 21218, USA*
[3]*APS Division, Department of Physics and Astronomy, Queen's University Belfast, Belfast BT7 1NN*
[4]*SUPA, School of Physics & Astronomy, University of St Andrews, North Haugh, St Andrews, Fife KY16 9SS*
[5]*University of Florida, PO Box 112005, 211 Bryant Space Science Centre, Gainesville, FL 32611-2055, USA*
[6]*Astrophysics Group, School of Chemistry & Physics, Keele University, Staffordshire ST5 5BG*
[7]*Las Cumbres Observatory, 6740B Cortona Drive, CA 93117, USA*
[8]*Department of Physics, Broida Hall, University of California, Santa Barbara, CA 93106-9530, USA*
[9]*Department of Physics & Astronomy, University of Leicester, Leicester LE1 7RH*
[10]*Institute of Astronomy, University of Cambridge, Madingley Road, Cambridge CB3 0HA*
[11]*Isaac Newton Group of Telescopes, Apartado de correos 321, E-3700 Santa Cruz de la Palma, Tenerife, Spain*
[12]*Department of Physics, University of Warwick, Coventry CV4 7AL*

Accepted 2007 July 27. Received 2007 July 27; in original form 2007 March 2

ABSTRACT

The Wide Angle Search for Planets (WASP) photometrically surveys a large number of nearby stars to uncover candidate extrasolar planet systems by virtue of small-amplitude light curve dips on a $\lesssim$5-d time-scale typical of the 'Hot-Jupiters'. Observations with the SuperWASP-North instrument between 2004 April and September produced a rich photometric data set of some 1.3×10^9 data points from 6.7 million stars. Our custom-built data acquisition and processing system produces $\sim$0.02 mag photometric precision at $V = 13$.

We present the transit candidates in the 03^h–06^h RA range. Out of 141 895 light curves with sufficient sampling to provide adequate coverage, 2688 show statistically significant transit-like periodicities. Out of these, 44 pass a visual inspection of the light curve, of which 24 are removed through a set of cuts on the statistical significance of artefacts. All but four of the remaining 20 objects are removed when prior information at higher spatial resolution from existing catalogues is taken into account. Of the four candidates remaining, one is considered a good candidate for follow-up observations with three further second-priority targets. We provide detailed information on these candidates, as well as a selection of the false-positives and astrophysical false-alarms that were eliminated, and discuss briefly the impact of sampling on our results.

Key words: methods: data analysis – planetary systems – stars: variables: other.

1 INTRODUCTION

The discovery of radial velocity variations indicative of a close planetary companion to 51 Peg (Mayor & Queloz 1995) caused a revolution in studies of planetary formation and evolution, as planets were traditionally thought not to exist as close as 0.05 au to the parent star (Pollack 1996). Subsequent radial velocity searches have uncovered 248 extrasolar planets (as of this writing)[1] orbiting main-sequence objects (e.g. Udry et al. 2000). Many of these systems comprise a population with periods typically $<$4 d and orbital separations of the order of 0.05 au, and this was an early challenge to theories of planet formation and evolution.

⋆E-mail: clarkson@stsci.edu

[1] http://exoplanets.eu/catalog.php

Transits combined with radial velocity measurements offer the only method to probe the internal structure of the exoplanets as they allow the planetary radius and mass to be determined. Twenty-two transiting extrasolar planets[2] now have reported mass and radius estimates (Bakos et al. 2007b; Burke et al. 2007; Charbonneau et al. 2007b; Torres et al. 2007), and although the number of systems is still low, the emerging picture is of a 'main sequence' of gas giants along the $\bar{\rho} \sim 1.0\,\mathrm{g\,cm^3}$ line at masses $\gtrsim 1 M_J$, and a second, more diverse population at lower mass but possibly inflated radius (e.g. Bakos et al. 2007a).

Studies of transiting exoplanets are driving current planetary formation and disc-migration theory. χ^2-fitting of physically motivated light curve models to the transit light curve allows joint constraints on the orbital inclination and planetary radius as a fraction of the stellar radius. The inclination estimate from the transit fitting then allows the planetary mass to be estimated directly from radial velocity measurements (e.g. Moutou et al. 2006). The accuracy to which the planetary radius itself can be determined is limited both by the photometric precision of the light curve and by the precision of the stellar radius determination. The latter is typically the limiting factor for space-based photometry (Brown et al. 2001).

2 INSTRUMENTATION AND OBSERVATIONS

2.1 Instrumentation

SuperWASP-North (hereafter SW-N) was the first multicamera WASP instrument to enter operation. Full details can be found in Pollacco et al. (2006); we summarize here the features relevant to this work. During 2004, the SW-N facility consisted of five wide-angle ($7.^{\circ}8 \times 7.^{\circ}8$ field of view) cameras on a rapid-slew fork-mount that allows overheads (for slew and settling between exposures) to be as short as 30 s even for slews $\gtrsim 8^{\circ}$. The 2048×2048-pixel detectors yield a plate-scale $\simeq 13.7$ arcsec pixel^{-1}, requiring careful consideration of the field location and observation depth to avoid washout by crowding. In 2004, the detector was unfiltered to maximize throughput, with an instrumental bandpass covering most of the Johnson *VRI* range, with blue and red cut-offs at 4000 and 10 000 Å, respectively. While the mount pointing error is at most 2 pixel rms across the sky, a slight misalignment of the instrument polar axis leads to a position drift of $\sim$10 pixel during the night.

2.2 Observational strategy

The WASP survey was planned around a broad-but-shallow approach to maximize planet yield, as this brings three key benefits when searching for exoplanet transits.

(i) *Further exoplanet diagnostics.* Detectable planetary transits offer the possibility of probing the atmosphere of the transiting planet. Charbonneau et al. (2006) list seven further constraints that can be made on a transiting planet–star system, but *only* if the parent star is sufficiently bright to allow high enough signal-to-noise ratio (S/N), including the setting of upper limits on atmospheric absorption features (Deming et al. 2005b), the setting of constraints on the vertical extent of the atmosphere by atomic species (Charbonneau et al. 2002; Vidal-Madjar et al. 2004), the search for spectroscopic features from the planet itself during secondary eclipse (Richardson, Deming & Seager 2003) and direct detection of thermal emission from the planet itself (Deming et al. 2005a). For the scientific return of transiting exoplanets to be fully realized, ground-based transit surveys such as WASP are typically optimized for objects at $V \lesssim 13$.

(ii) *Facility of follow-up observations.* One of the byproducts of the OGLE microlensing project was a set of objects showing apparent characteristics of exoplanet occultation ($P_{\mathrm{orb}} \sim 1$–10 d, flux removal $\Delta F/F \sim 1$ per cent, event duration $\sim$ hours; Udalski et al. 2002a,b,c). Strenuous follow-up spectroscopic observations by several groups (e.g. Bouchy et al. 2005) showed that a high fraction of these objects were astrophysical false-alarms such as grazing-incidence stellar binaries or a large-amplitude variable blended with the brighter target. Dedicated narrow-deep photometric surveys (with e.g. *HST* or the upcoming *Kepler* mission) afford such high coverage and spatial resolution that this class of astrophysical false-alarms can be minimized to high confidence from the photometry alone (to the level where <1 astrophysical false-positive is expected from the entire survey e.g. Sahu et al. 2006). For ground-based surveys, however, the astrophysical false-positives will, for the foreseeable future, be a large and important class of candidates; a population study using the Two-Micron All-Sky Survey (2MASS) catalogue suggests an *astrophysical* false-alarm-to-transit ratio of at least 10:1 (Brown 2003); ground-based follow-up observations are thus still essential. At the time of survey planning, a consideration of a variety of ground-based photometric observing strategies [in the presence of uncorrelated ('white') noise; Horne 2003] suggested that the SW-N hardware would provide survey statistics competitive with all other existing transit surveys while avoiding excessive crowding at fainter magnitudes. The SW-N limiting magnitude to transits of $V \sim 13$ (with 30-s exposures) allows follow-up observations to take place with approximately one-tenth the exposure time (or collecting area) as similar observations of OGLE candidates (themselves in the range $15 \leqslant V \leqslant 21$; Udalski et al. 2002a).

(iii) *Catalogue-based elimination of Astrophysical False-positives.* With the availability of the USNO-B1.0 (hereafter USNO), Tycho-2 and 2MASS catalogues, multicolour absolute magnitude estimates already exist at higher spatial resolution than the programme variability observations. Tycho-2 is $\sim$90 per cent complete down to $V \simeq 11.5$ mag (Høg et al. 2000), while comparison with the Sloan Digital Sky Survey suggests that USNO is 97 per cent complete for stars out to $g' \sim 20$ (roughly Johnson $B \sim 20$; Monet et al. 2003). This allows obvious astrophysical false-positives to be eliminated during analysis of the photometry; for the fields we report here, roughly 77 per cent of photometrically promising candidates are ruled out in this manner before any follow-up observations take place.

30-s snapshots of each field of view are taken in sequences of eight surrounding the Meridian; once the sequence is complete, the camera returns to the start of the sequence for the next run. The rapid-slew capability of the mount allows a cadence of $\simeq$9 min per field. Fields centred at declination $+23^{\circ} \leqslant \delta^{\circ} \leqslant +32^{\circ}$ were generally chosen to provide optimal survey grasp without crowding washout, though with Galactic plane avoidance some fields at other declinations were sampled (see Pollacco et al. 2006).[3] As the westernmost field in the group of eight moves to high airmass, this field is abandoned and a new field is added on the east. The net result is a

[2] Including the two transiting exoplanets WASP-1b and WASP-2b, which were discovered in other fields from the 2004 WASP survey (Collier Cameron et al. 2007).

[3] The full range of declinations imaged including Galactic plane avoidance is thus $(+12^{\circ} < \delta^{\circ} < +47^{\circ})$.

light curve with ∼9-min cadence, consisting of roughly 35 frames per night for well-sampled fields. As the sky precesses throughout the year, roughly 60 nights' data are collected for each field for each camera.

3 ANALYSIS TECHNIQUES

We outline briefly the analysis techniques used in this project. The reduction and detection procedures are described more fully in Pollacco et al. (2006) and Collier Cameron et al. (2006), see also the companion papers in this series (Christian et al. 2006; Lister et al. 2007; Street et al. 2007).

3.1 Photometry pipeline

The collaboration has built a fully automated data-reduction pipeline that achieves our goal of obtaining photometric precision of ∼1 per cent for stars with $V < 13$. Photometric precision is typically 0.02 mag at $V = 13$, with 5 mmag achieved at $V = 8.5$. The pipeline uses custom-written f77 programs and several STARLINK packages called from shell scripts; it is thus somewhat portable and uses capabilities already freely available as much as possible. The pipeline itself is described more fully in Pollacco et al. (2006); here we remark on its following relevant features.

(1) Frame classification and quality control is performed on the input frames through statistical characterization of the frame content, with minimal reliance on object headers. Currently, ∼85 per cent of frames are accepted for further processing depending on the observing conditions during any given night.

(2) Running calibrations are produced by optimally weighting the calibration history across a season, including exponentially decreasing weighting with a 14-d time-scale to allow for varying dust patterns on the lens and other systematics which can vary with time. This measurably reduces the systematic scatter in the thermal, flat-field and bias frames.

(3) By triangle-matching selected detected objects with *Hipparcos* positions in the Tycho-2 catalogue, a full nine-term plate solution on the tangent plane is derived, allowing for pointing errors and distortion within the glass of the lens by fitting observed stellar positions directly to their catalogued positions on the sky.

(4) Objects are detected in the frame at $>4\sigma$ above background (using a modified version of SEXTRACTOR; Bertin & Arnouts 1996). Dedicated f77 routines produce aperture photometry in three concentric apertures of radius 2.5, 3.5 and 4.5 pixel. Light curves using the 3.5-pixel aperture are retained for further processing; a variant of the curve-of-growth method of Stetson (1990) is used to affix a blending index to each object based on the flux evolution with aperture size.

(5) Light curves from a given field are processed as an ensemble to fit the transformation from the instrumental magnitude system to the Tycho-2 V bandpass. The data are weighted using inverse variance weights that incorporate, in addition to the formal errors from the pipeline, variance components that quantify the intrinsic variability of each star and the patchiness of extinction across each frame. These additional variances are estimated using the maximum-likelihood method described by Collier Cameron et al. (2006). The magnitude zero-point is determined to a precision of 1–2 mmag per frame (Collier Cameron et al. 2006; Pollacco et al. 2006).

(6) The photometry is then uploaded to the WASP archive at the Leicester University, which allows rapid access to time-series of various quantities for each object, through a custom-written query language based on SQL.

3.2 Photometric transit candidates

At this stage, small systematic trends are still present in the photometry; nevertheless, we store these data in the archive rather than storing detrended data. It was envisaged that detrending routines would improve over time; this approach thus allows the user to apply the latest, best routines at the analysis stage. For the work described here, the generalized linear trend-removal algorithm SYSREM (Tamuz, Mazeh & Zucker 2005) was employed to remove the remaining systematic trends. Investigation is currently underway to fully characterize these trends for future data sets. Under the nominal observing strategy, 35 frames per night are taken for well-sampled fields; however, because not all fields are well sampled under an automated run (e.g. a field might have only a few frames taken before dawn), we cannot assume that all objects are well sampled. Objects were selected for further analysis for the transit search if at least 500 points were recorded over more than 10 nights, with Tycho-2 $V \lesssim 13$.

The resulting set of light curves were subjected to automated application of transit-detection algorithms to isolate the small subset of transit candidates. A comparison of the matched-filter (Street et al. 2003), box least-squares (Kovács et al. 2002; hereafter BLS) and Bayesian back-end (Aigrain & Favata 2002) techniques suggests that a BLS technique is most suited to our purposes (Aigrain & Irwin 2004), and so was selected as our main transit-search algorithm. Our own Monte Carlo simulations of the effectiveness of the transit algorithms when applied to artificial transits over real noise light curves from WASP will be reported elsewhere (Enoch et al., in preparation). The BLS algorithm was implemented in a two-stage process. An initial coarse-grid search was made over the period range ($0.9 \leqslant P \leqslant 5$ d), with the period range chosen to allow for some exploration of period space beneath the 1-d boundary, while still producing well-sampled light curves at the long end of the period range. The period interval is set to ensure distinguishable folded light curves, in the sense that when folded on two successive periods in the interval, the resulting phase difference of a given feature between the two light curves corresponds to the expected transit width at the longest period searched. The results of this coarse pass were refined by a second, finer pass in which the period spacing is now set so that the phase drift over the entire data set is less than *half* the expected transit width (Collier Cameron et al. 2006). A typical period spacing would thus be 0.002 d for the coarse search and 0.001 d for the finer search. For each candidate, fit statistics and parameters of the best-fitting transit model at this stage were obtained for the five most significant period detections. Detections were ranked by the fit statistic $\Delta\chi^2$, which gives the improvement of the best-fitting transit model over a flat light curve model, and is our adopted proxy for the transit S/N detection.

Filtering of the candidate list was then applied based on: (i) repetition of a transit-like event, (ii) reduced χ^2-statistic of the best-fitting transit model $\chi^2_\nu < 3.5$, (iii) the presence of any gaps in the folded transit light curve a factor of >2.5 longer than the transit width – indicative of a fit dominated by sampling gaps, (iv) the S/N in the presence of correlated noise (commonly called 'red-noise') $S_{\rm red}$ (Pont, Zucker & Queloz 2006), and (v) the transit-to-anti-transit ratio $\Delta\chi^2/\Delta\chi^2_-$. The latter measures the improvement in fit-statistic $\Delta\chi^2$ when a transit model consisting of regular intensity dips is fitted, scaled by the improvement $\Delta\chi^2_-$ when an 'anti-transit' model consisting of regular flux *brightenings* is fitted instead. This

statistic can be used to characterize light curves with a strong correlated noise component (Burke et al. 2006).

Correlated noise introduces significant systematics which raise the detection threshold for significant periodicities in time-series data. Although well characterized in several fields in astrophysics (such as X-ray-variability studies; e.g. Homer et al. 2001), its relevance to optical searches for exoplanets was not fully appreciated when the ground-based transit surveys were planned, and thus deserves some amplification here (see also the discussion, Smith et al. 2006; Collier Cameron et al. 2006). For ground-based photometric surveys, the errors in measurement are usually correlated on time-scales of tens of minutes to hours, producing a low-frequency component to the noise that can mimic an exoplanet transit. $N_{\rm tr}$ transits are observed, with L_i measurements in each transit. The transit is assumed to be a step-function to the photometric precision of SW-N so that each data point observed during transit is treated as an estimate of the full transit depth δ. These estimates are binned by a transit number, with corresponding binned measurement error $\sigma_{{\rm bin},i}$. The S/N estimate for the full set of transit measurements is then

$$S^2_{\rm red} = \sum_{i=1}^{N_{\rm tr}} \frac{\delta_i^2}{\sigma^2_{{\rm bin},i}(L_i)}. \quad (1)$$

We require a prescription for the relation between the binned measurement error $\sigma_{\rm bin}$ and unbinned error $\sigma_{\rm u}$ in the presence of real noise. In the case of SW-N data, this relationship is characterized as

$$\sigma_{\rm bin} = \sigma_{\rm u} L^b. \quad (2)$$

Pure uncorrelated noise would show the familiar $b = -0.5$ while binning would not improve matters for fully correlated noise and thus $b = 0$. For each star, out-of-transit data from each night are used to estimate the index b from a fit to $\sigma_{\rm bin}/\sigma_{\rm u}$ as a function of L. The relation (2) is then used to relate the unbinned rms scatter observed during transit $\sigma_{{\rm u},i}$ to the rms scatter of the binned estimate of the transit depth. In reality, L_i and b will vary on a night-by-night basis; in order to filter on a star-by-star basis, we take the average values of L and b across the observed transits, leading to

$$S_{\rm red} = \frac{\delta\sqrt{N_{\rm t}}}{\sigma_{\rm u} L^b}, \quad (3)$$

where the rms scatter of the unbinned data $\sigma_{\rm u}$ is now taken across all the data points during transit. Further information is given in Collier Cameron et al. (2006); note that for objects with $V < 11$ the covariance parameter b is not quite -0.5 after detrending, which suggests that a low level of residual structure may be present in the detrended light curves.

We remind the reader that we are ranking periodicities from each candidate by several criteria in the same search, so care must be taken to interpret the ranking that results. In two cases, the attempt by the algorithm to maximize S/N in the presence of correlated noise $S_{\rm red}$ caused the returned best-fitting period to jump to a shorter period that was much less significant than the most-significant trough in the BLS periodogram. The $S_{\rm red}$ statistic can become very low at certain pathological frequencies which beat with the day–night cycle, producing a much higher-than-average number of observable transits. Even if the $\Delta\chi^2$ is not highly significant at such frequencies, $S_{\rm red}$ can thus become very large. $S_{\rm red}$ is therefore only used to determine whether the frequencies associated with the strongest $\Delta\chi^2$ actually yield significant detections when the contribution from correlated noise is considered.

Detections with the five highest $S_{\rm red}$ values are produced for each candidate; where the best detections show similar $S_{\rm red}$, we retained the detection corresponding to the most-significant trough in the BLS periodogram (e.g. the candidate J025922.67+275416.0). In one case, the most-significant trough in the BLS periodogram only sampled two transits, so we rejected that period and chose the second strongest (J051849.56+211513.6). In most cases, the most-significant detection in the BLS periodogram was clearly much more significant than its nearest rivals (see Fig. 2); however, in at least one case several marginally less significant period detections were also reported (J051849.56+211513.6; Section 4); no account was taken of these secondary detections in this case.

The result is a set of 2688 transit candidates ranked by the fit-statistic $\Delta\chi^2$. The light curves and BLS periodograms for each of these objects were visually examined, to remove light curves dominated by obvious sampling effects and other artefacts. This examination was carried out independently by the first two authors and the final list was produced after a comparison of the analyses. Objects are deselected from further consideration if their light curves meet any two of the following criteria.

(1) Folded light curve dominated by sampling gaps.
(2) Most significantly detected period and the nearest alias of the 1D sampling are indistinguishable from each other in the BLS periodogram.
(3) Visible out-of-transit variability both above and below the mean flux level.
(4) Photometric transit-depth, δ, greater than 15 per cent.
(5) Deep, V-shaped light curve suggestive of stellar transit.[4]
(6) Ellipsoidal trends apparent in folded light curve.
(7) Multiple transit events are apparent in the folded light curve, suggesting that an incorrect period has been used, and the corrected period is outside the 0.9–5 d period range.
(8) Transit duration greater than 5 h.
(9) Only two apparent transit events present in the entire light curve (if a candidate meets this criterion, then it is removed from further consideration).

This visual inspection trimmed the 2688 candidates further to 44, comprising 20 targets considered likely from the photometry to contain a transiting extrasolar planet (Priority 1) and 24 candidates where just one of the above tests is failed by the candidates (Priority 2 candidates). At this stage, a number of cuts were made on the surviving objects based on light curve statistics returned from the period-search and light curve analysis. Objects were only passed forward as candidates if:

(1) S/N in the presence of correlated noise $S_{\rm red} > 8$ (cf. Pont et al. 2006).
(2) Period $\geqslant$1.05 d.
(3) S/N of ellipsoidal variations $<$8.0 (cf. Sirko & Paczyński 2003).
(4) Transit to anti-transit ratio $\Delta\chi^2/\Delta\chi^2_- \geqslant 2.0$ (cf. Burke et al. 2006).

All but 20 of the remaining candidates were filtered out by these steps. In summary, then, a typical field would contain several hundred raw candidates, out of which a visual inspection would leave one to two Priority 1 and three to four Priority 2 candidates; however further cuts against correlated noise, ellipsoidal variations and period would reduce this number by about half (see Table 1).

[4] This criterion was used for objects with $\gtrsim$10 per cent intensity dips that are clearly stellar binaries; more marginal cases are retained as possible exoplanet candidates.

Table 1. Field statistics. For each field, we report (i) $N_{\rm cand}$ – the number of targets selected for the BLS search algorithm, (ii) $N_{\rm hun}$ – the number of candidates passed forward for visual selection, and (iii) $N_{\rm vis}$ – the number of candidates passing a visual selection (Priority 1/Priority 2), (iv) $N_{\rm S/N}$ – the number of candidates passing further cuts against short periods, ellipsoidal variations and noise signatures (Priority 1/Priority 2), (v) $N_{\rm f}$ – final number of candidates (Priority 1/Priority 2).

RA	Dec.	Nights	Frames	$N_{\rm cand}$	$N_{\rm hun}$	$N_{\rm vis}$	$N_{\rm S/N}$	$N_{\rm f}$
0316	+3126	60	1882	6810	162	3/5	1/0	0/1
0317	+2326	60	1885	5942	161	3/1	3/0	0/1
0343	+3126	64	1402	8465	115	0/1	0/0	0/0
0344	+2427	27	607	6037	136	0/0	0/0	0/0
0344	+3944	46	1402	17 615	417	0/1	0/1	0/0
0416	+3126	46	1400	11 106	231	2/1	1/0	0/0
0417	+2326	46	1357	6241	117	0/0	0/0	0/0
0443	+3126	44	1029	8314	147	2/1	2/0	0/0
0444	+3944	43	1014	20 432	368	0/1	0/0	0/0
0516	+3126	43	1008	22 406	389	5/5	4/2	1/0
0517	+2326	43	1013	13 506	219	1/5	1/4	0/1
0543	+3126	37	524	15 021	226	4/3	1/0	0/0
			Totals	141 895	2688	20/24	13/7	1/3

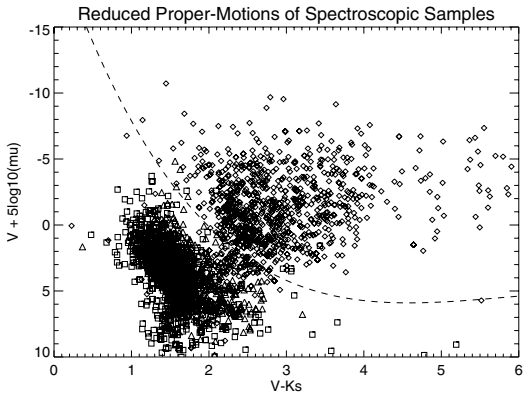

Figure 1. Reduced proper motion versus $(V-K_{\rm S})$ colour of a selection of giants and dwarfs from the Cayrel de Strobel et al. (2001) and Valenti & Fisher (2005) surveys (using proper motions in mas yr^{-1}). Diamonds: Cayrel et al. giants. Boxes: Cayrel et al. dwarfs. Triangles: Valenti & Fischer dwarfs. The dashed line shows a polynomial boundary (as a function of $V_{\rm SW}-K_{\rm S}$) constructed to discriminate between the two regions. This boundary serves as a guide for automatic classification; however, the position of each photometric transit candidate was visually checked in this diagram for assessment of luminosity class.

3.3 Catalogue-based assessment

The final cut is the use of prior knowledge from previous surveys with higher spatial resolution and multi-filter information to remove surviving systems that are likely to be blends or other astrophysical false-positives. This stage cuts the list of candidates still further.

As we remarked in Section 2.2, the depth of the 2MASS, Tycho-2 and USNO surveys allows the suitability of the remaining candidates to be assessed on the basis of their colours and proximity to potential photometric crowding objects. A custom-built online query tool was implemented by the Consortium to query a variety of astronomical catalogues at the position of the transit candidates, returning survey images of the target field and multiwavelength information for the target and nearby objects from which the parent stellar parameters can be estimated. We refer the reader to Wilson et al. (2006) for more detailed information on this process.

(i) *Luminosity class and spectral type.* As pointed out by Gould & Morgan (2003), roughly 90 per cent of the bright stars surveyed by ground-based exoplanet transit searches are giants for which a transiting exoplanet would produce well under 1 per cent dips; this predicts a rather high astrophysical false-positive rate (Brown 2003). Stellar populations in the Galactic disc show coherent, restricted velocity distributions (e.g. Binney & Merrifield 1998). The reduced proper motion (RPM) can be used to kinematically segregate members of nearby stellar populations; in particular, its correlation with absolute magnitude allows WASP targets with proper motions (available from the USNO catalogue for most objects) to be roughly classified by a luminosity class. The position of the target in the $\{{\rm RPM}–(V-K_{\rm S})\}$ space is determined using the Tycho-2 V magnitude (using the observed SuperWASP V magnitude $V_{\rm SW}$ as a check), catalogue $K_{\rm S}$ and proper motion estimates from the USNO catalogue. The luminosity class division is based on spectroscopic surveys of a number of nearby objects, in particular the Cayrel de Strobel, Soubiran & Ralite (2001) catalogue and the Valenti & Fisher (2005) catalogue from the N2K survey, with the luminosity class estimated with reference to this fit (Fig. 1). Unknown reddening is, in principle, a systematic bias with this measure, as it causes the observed $(V-K_{\rm S})$ and RPM both to be artificially higher than the intrinsic properties.

The RPM diagnostic was checked manually for cases in which it was in anyway ambiguous; in particular, the $\{{\rm RPM}, (V-K_{\rm S})\}$ diagnostic becomes somewhat inconclusive for objects with *both* $1.5 \lesssim (V-K_{\rm S}) \lesssim 2.2$ and RPM $\lesssim 2$ (Fig. 1). Estimates of the astrometric accuracy of stellar positions on the plates used, combined with transformation errors, produce a quality flag in USNO that gives a probability estimate of the reported proper motion being correct (Monet et al. 2003). Low values of this quality flag suggest a poor proper motion measurement. We also use the flux–angular diameter relation from interferometric studies (Kervella et al. 2004; Foqué & Gieren 1997); given catalogue $B, K_{\rm S}$ magnitudes, the angular diameter can be inferred and converted into stellar radius using the *Hipparcos* parallax (if available) to infer distance. If the available information is ambiguous as to the luminosity class of a target, it is reduced in priority.

(ii) *Stellar radius.* For main-sequence stars, the transit depth combined with the 2MASS $(J-H)$ colour also provides an estimate for the spectral type and radius of the parent star, and thus the radius of the putative planet (Ammons et al. 2006). Note that because Ammons et al. (2006) also used 2MASS photometry, transformation from 2MASS into, for example, the Bessell & Brett (1988) system is not required to estimate radii, removing a potential source of systematic error. For dwarfs, the $(J-H)$–radius relationship suffers from a degeneracy, in that the relationship turns over at spectral type ∼M0 (Bessell & Brett 1988). As a cross-check, we use $(V-K_{\rm S})$ and $(B-V)$ to estimate effective temperature (Blackwell & Lynas-Gray 1998a,b), and the radius from the standard temperature–radius relation for main-sequence stars (Gray 1992). B magnitudes for this step are taken from USNO, V from Tycho 2 or, if unavailable, from SW-N. The observed transit depth is used to estimate the planetary radius assuming that the occultation is due to the full disc of the planet at a maximum depth. $(V-K_{\rm S})$ colours also provide a way to break the $(J-H)$–radius degeneracy; should an object show observed $(V-K_{\rm S})$ too blue for an M0 dwarf, the $(J-H)$ colour must correspond to spectral type earlier than M0 – in practice, this applies for all the candidates presented here.

SW-N routinely achieves photometric precision ∼5 mmag at $V = 8.5$, rising to 0.02 mag at $V = 13$; Tycho-2 shows photometric error ∼0.05 mag at $V = 10.0$–11.0, rising to 0.11 mag at $V = 11.0$–12.0 (Høg et al. 2000). 2MASS observations of calibration standards show rms residuals of the order of $\gtrsim$0.05 mag in the ($10 \leqslant H \leqslant 14$) range (Nikolaev et al. 2000; Carpenter 2001), so we may expect photometric errors to be comparable to reddening effects for comparatively high reddening. For example, with absolute magnitude $M_V \sim 4$, a typical late-F/early-G dwarf located roughly 200 pc from the Sun would be measured at Tycho-2 $V \sim 10.5$ mag. For the fields of interest here, the local H I column density out to this distance is of the order of 10^{20} cm^{-2} (Fruscione et al. 1994), leading to reddening $E(B-V) \sim 0.02$ and extinction $A_V \sim 0.06$ (cf. Binney & Merrifield 1998). Thus, a subset of objects in the survey will show uncertain extinction in V that is comparable to the photometric uncertainty associated with $(V - K_S)$. We thus use parameters inferred from the 2MASS $(J - H)$ colour preferentially over $(V - K_S)$ when the two measures disagree.

The most-inflated planet currently known has radius $R \sim 1.44 R_J$ (Charbonneau et al. 2007a), so we regard SW-N candidates with inferred radii $\lesssim 1.5 R_J$ as sensible candidates. However, we do not reject outright candidates with slightly larger inferred radii to allow for photometric uncertainty in this detection survey.

Finally, we compute, but do not use as a selection criterion, the ratio of observed transit width to that predicted, given best-fitting stellar parameters, $\eta = W_{obs}/W$. In principle, we expect genuine exoplanet transits to show $\eta \sim 1$, with some range in values due to observational scatter and inclination variations. This figure of merit was introduced and computed for the OGLE transit candidates by Tingley & Sackett (2005); in practice, all genuine OGLE transiting planets show $0.5 \lesssim \eta \lesssim 1$.

(iii) *Positional matching.* We also visually check the positions localized by the SW-N pipeline against catalogue position for the target used by the automated query tool; in a few cases, the measured position was displaced by a small amount from the catalogue position (even subpixel offsets can amount to nearly 15 arcsec; Section 2.1). Even assuming perfect distortion correction in the pipeline and no error introduced in the conversion of positions between epochs in the catalogues, objects with high proper motion may have drifted appreciably in the two to three decades since some of the catalogue observations were made. In cases where an object is detected at a slightly different location from its catalogue position, the automated catalogue query tool can misidentify the target as a blending neighbour. In these cases, we use the measured magnitude V_{SW} to determine the most likely matching catalogue object, and re-calculate the diagnostics accordingly.

(iv) *Crowding.* Candidates were rejected outright if any object brighter than the candidate was present within the 48-arcsec SW-N aperture. For candidates with nearby objects *fainter* than the candidate, we calculate the magnitude of the nearby object that would be required for a 50 per cent depth eclipse from the object to produce the observed transit depth from the aperture; if this magnitude is surpassed, the candidate is rejected.

4 RESULTS

The bottom line of this analysis is that one out of 2688 candidates is put forward as a Priority 1 target for spectroscopic follow-up with three out of the 2688 Priority 2 targets. Table 1 gives the field statistics for the search. Table 2 lists the 44 objects surviving a visual inspection. Table 3 gives the four candidates finally accepted. We provide notes on the accepted objects below, as well as a subset of the rejected candidates. Some of the rejected objects are of interest in their own right, either because their rejection is illustrative of the procedures we followed to filter out candidates, or because the objects are astrophysically interesting (Section 4.3).

4.1 Priority 1 candidate

Only one object assigned Priority 1 on the basis of the visual and S/N cuts (Section 3.2) survived the application of catalogue information. See Fig. 2 for its light curve and BLS periodogram.

(i) *1SWASP J051221.34+300634.9.* This object shows an almost prototypical transit candidate event of 3 per cent depth over a flat out-of-transit light curve. Five transits are observed with a 1.24-d period and 1.87-h transit duration. With RPM 2.19 and $(V - K_S) = 1.61$, this object is firmly in the dwarf regime (Fig. 2). Two USNO objects are $\gtrsim$4.37 mag fainter than the target within the 48-arcsec SW-N aperture, and thus are too faint to produce blending at the detected transit level. 2MASS $(J - H) = 0.26$ suggests a 1.15-$R_\odot$ F9 primary, implying the planet radius $1.71 R_J$ and Tingley & Sackett $\eta = 0.77$.

4.2 Priority 2 candidates

Two objects were initially assigned Priority 1 from a visual analysis and the S/N cuts in Section 3.2; however, inclusion of prior information from catalogues highlighted some uncertainty in the luminosity class of these objects, thus they were demoted to Priority 2. One further object that was initially assigned Priority 2 survived the inclusion of catalogued information. Periodograms and light curves for all three objects can be found in Fig. 3.

(i) *1SWASP J031103.19+211141.4.* Deep (4.03 per cent), clearly visible transit events are present, though there may be some structure in the transit besides a planetary-type event. No Tycho-2 or *Hipparcos* objects are found at the object position or within a 48 arcsec radius, making stellar radius determination using the apparent diameter relations of Kervella et al. (2004) impossible. USNO lists no potential blends within the SW-N aperture. The luminosity class of this object is somewhat open to question. USNO reports a bad measurement for proper motion, so the RPM has nothing to say about the luminosity class of this object (at $V - K_S = 1.88$ this measure would be ambiguous for this object for proper motions $\lesssim$8 mas yr^{-1}).
Assuming that the parent star is of luminosity class *V*, 2MASS $(J - H) = 0.27$ implies parent spectral type G0 and radius $\sim 1.12\,R_\odot$. This implies a planetary radius $\sim 1.89 R_J$, with the Tingley & Sackett figure of merit $\eta = 0.94$, just within the range corresponding to likely exoplanet transits (Tingley & Sackett 2005).

(ii) *1SWASP J032739.88+305511.3.* This object shows a clear shallow transit-like event (2.53 per cent), on a 1.05 d period clearly distinct from the 1-d trough in the periodogram (Fig. 3); at this period, 14 transits are observed. No *Hipparcos* or Tycho-2 objects are found at the target position or within 48 arcsec of the target, so direct inference of the stellar radius (cf. Kervella et al. 2004) is not possible. USNO lists no potential blending objects within the SW-N aperture. As with J031103.19+211141.4, the USNO proper motion measurement cannot be used due to poor quality (Section 3.3). However, with $(V - K_S) \sim 2.9$, this object would have to show proper motion $\gtrsim$15 mas yr^{-1} to be close enough to be a likely dwarf (Fig. 1), which is rather high to go unnoticed over the 25-yr time base of the USNO catalogue. Thus, there is the suspicion that this object may be a giant and it was thus demoted to Priority 2. Colour index 2MASS

Table 2. Candidates from the BLS search that pass an initial visual inspection. N_{tr} denotes the number of transits observed, n_t the number of valid observations of the object, n the number of valid points during transit, $\Delta\chi^2$ the improvement of the best-fitting transit model over a flat light curve model, $\Delta\chi^2/\Delta\chi^2_-$ the ratio of this fitting statistic when using the transit model to an 'anti-transit' brightening model (Section 3.3), S_{ell} the S/N of ellipsoidal variation, S_{red} the S/N including correlated noise. The final two columns give the priority according to the candidate at the stage of the visual examination and the primary reason for its rejection (if applicable). Reasons for removal are: low S/N against correlated 'red' noise (R), presence of ellipsoidal variations (E) and low $\Delta\chi^2/\Delta\chi^2_-$ (A).

SWASP ID	Period (d)	Duration (h)	Depth (mag)	N_{tr}	n_{pts}	n	$\Delta\chi^2$	$\frac{\Delta\chi^2}{\Delta\chi^2_-}$	S_{ell}	S_{red}	Vis	Cut
J025922.67+275416.0	1.098 797	2.38	0.0179	8	1693	129	154.226	2.734	1.051	6.923	P2	R
J025947.03+283310.4	3.074 289	4.61	0.0132	5	1694	80	219.119	2.826	3.298	7.335	P2	R
J030117.53+274943.0	3.070 961	3.86	0.0241	4	1693	64	103.562	1.661	1.416	6.936	P2	R
J030153.95+332213.0	2.350 089	5.18	0.0450	12	1694	228	660.272	4.386	0.399	7.321	P2	R
J031632.80+300144.2	2.198 882	3.29	0.0310	6	1692	112	1457.156	5.896	25.784	14.364	P1	E
J032515.17+341031.6	1.011 542	3.29	0.0374	17	1693	300	582.241	4.481	6.685	11.121	P1	P
J032739.88+305511.3	1.051 158	3.00	0.0253	14	1693	234	911.154	5.764	2.966	9.758	P1	
J033503.83+325915.2	2.135 410	2.33	0.0650	9	1694	106	929.219	2.793	15.031	9.837	P2	E
J030157.61+204037.1	1.571 295	3.17	0.0807	9	1690	144	2213.008	37.633	3.246	12.431	P1	
J030854.44+234517.4	2.206 365	4.25	0.0567	7	1434	101	616.065	8.403	6.469	16.135	P1	
J031103.19+211141.4	2.730 148	3.46	0.0403	5	1690	89	712.650	12.847	5.348	9.077	P1	
J033042.00+243027.9	3.178 541	3.98	0.0157	3	1690	72	613.552	10.072	11.575	6.354	P2	R
J034747.35+350105.7	1.928 731	2.16	0.0254	5	1267	163	2847.39	11.321	13.692	7.533	P2	R
J034628.00+365747.0	1.856 870	2.33	0.0703	3	1242	63	736.339	16.640	0.877	8.105	P2	
J041411.76+302105.0	2.554 799	4.58	0.0565	6	1312	115	1349.406	17.297	6.050	9.292	P1	
J042255.90+290701.5	2.054 940	1.80	0.0680	6	1312	138	2083.12	6.685	29.186	8.669	P2	E
J042518.63+305018.1	1.265 071	1.78	0.1036	8	1312	83	6393.781	9.069	11.243	10.328	P1	E
J045349.66+333842.5	1.843 365	4.27	0.0340	6	913	94	422.898	1.694	11.032	8.736	P2	A
J045441.00+335323.2	1.435 404	1.97	0.1118	5	913	45	871.943	10.557	2.699	11.698	P1	
J044803.38+342415.5	1.385 160	3.10	0.1202	7	913	102	1718.045	15.560	4.113	10.556	P1	
J050328.03+394509.4	1.727 674	2.16	0.0431	3	619	61	796.254	7.185	15.228	5.132	P2	R
J050712.55+335934.4	1.389 950	2.09	0.0195	6	826	72	351.477	7.992	1.392	8.023	P1	
J050917.50+300309.8	1.923 790	1.78	0.0274	5	826	114	373.920	2.815	7.905	6.973	P2	R
J051221.34+300634.9	1.237 851	1.87	0.0304	5	822	49	977.310	15.529	0.125	9.080	P1	
J051414.50+350639.9	1.659 918	2.47	0.1866	8	816	122	2770.867	14.260	12.015	9.692	P1	E
J051632.17+304921.5	2.558 843	5.83	0.0537	8	824	102	404.012	14.722	4.356	9.510	P1	
J052123.50+343759.3	1.911 629	2.14	0.1091	6	826	32	822.981	8.824	3.169	12.427	P2	
J052155.26+334037.0	1.820 449	2.35	0.0255	3	825	43	274.351	17.576	0.377	7.871	P2	R
J052155.29+311153.2	2.552 743	2.33	0.0172	4	823	46	112.207	8.394	0.599	10.579	P2	
J052639.24+341813.9	1.172 678	2.78	0.0843	6	826	74	4831.498	60.055	17.855	9.546	P2	E
J053442.52+312922.3	1.675 041	2.40	0.0857	3	826	38	2048.602	24.867	0.544	9.203	P1	
J050210.19+222523.8	1.968 182	2.78	0.0968	4	834	38	1338.312	7.930	5.896	12.496	P2	
J050241.49+235554.6	4.148 943	5.26	0.0753	3	834	40	755.581	6.135	1.365	9.933	P1	
J050642.37+214850.2	1.620 502	2.54	0.0857	3	834	35	1264.624	33.940	3.185	9.215	P2	
J051108.55+230632.3	1.709 274	2.59	0.0235	4	819	66	948.96	2.809	22.846	7.396	P2	E
J051109.87+222428.3	1.391 621	2.90	0.0306	5	834	68	310.172	3.820	3.518	8.258	P2	
J051849.56+211513.6	1.348 566	2.28	0.0579	6	834	57	211.862	4.363	1.103	13.136	P2	
J053026.87+350839.4	1.225 148	2.16	0.0668	5	524	50	512.587	20.940	5.471	7.767	P1	R
J053428.54+331646.7	1.227 779	4.99	0.0672	6	523	86	1357.361	19.554	0.455	7.339	P2	R
J053430.23+331610.6	1.229 169	4.73	0.0393	7	523	84	759.293	8.590	0.170	7.700	P1	R
J054511.65+323330.7	1.553 595	1.49	0.0486	3	519	20	507.882	9.426	1.155	11.655	P1	
J054645.34+292753.7	1.175 271	2.11	0.0620	3	512	31	414.517	1.839	3.775	13.211	P2	A
J055303.05+275339.4	2.410 921	3.34	0.0628	3	524	37	1552.535	15.285	4.518	6.238	P1	R
J055557.92+283738.4	1.241 766	2.66	0.0198	5	521	51	105.570	1.543	1.690	8.076	P2	A

$(J-H) = 0.22$ suggests a 1.23-$R_\odot$ parent with spectral type F8, *assuming* that it falls on the main sequence. This predicts a planet radius $1.69R_J$ and the Tingley & Sackett $\eta = 1.06$.

(iii) *1SWASP J051849.56+211513.6.* This object shows six transit-like events of ∼6 per cent depth on a 1.35-d period and with a 2.3-h transit duration. The transit light curve is rather deep and possibly V-shaped, however, consistent with a planetary transit, given the photometric precision (Fig. 3). With RPM ∼1.62 and $(V-K_S) = 2.2$, this object lies within a region of parameter space roughly equally populated by dwarfs and giants, thus its luminosity class is uncertain. *Assuming* that the parent star is a main-sequence object, the 2MASS colours $(J-H) = 0.27$ suggest a 1.12-$R_\odot$ G0 primary, implying a planetary radius of $2.3R_J$ and the Tingley & Sackett $\eta = 0.88$, so these parameters are consistent with a transiting exoplanet. In addition to the luminosity-class uncertainty for this object, the light curve shows possible variability at anti-transit,

Table 3. Light curve timing information for the candidates. HJD of mid-transit = 245 0000.0 + Epoch. η is the Tingley & Sackett figure of merit for identification with a transiting exoplanet (Tingley & Sackett 2005). Errors here and throughout this report are formal 1σ errors on transit model fits to the data.

SWASP ID	Epoch (d)	Period (d)	Duration (h)	Depth (per cent)	η	$N_{\rm trans}$	$V_{\rm SW}$
1SWASP J051221.34+300634.9	3218.6880 ± 0.0009	$1.2379 \pm 2.7 \times 10^{-5}$	1.872 ± 0.048	3.04 ± 0.09	0.77	5	10.90
1SWASP J031103.19+211141.4	3193.2342 ± 0.0023	$2.7301 \pm 1.03 \times 10^{-4}$	3.46 ± 0.12	4.03 ± 0.14	0.94	5	12.23
1SWASP J032739.88+305511.3	3194.3954 ± 0.0014	$1.0512 \pm 2.60 \times 10^{-5}$	3.00 ± 0.07	2.53 ± 0.08	1.06	14	12.17
1SWASP J051849.56+211513.6	3219.3183 ± 0.0024	$1.3486 \pm 6.20 \times 10^{-5}$	2.28 ± 0.12	5.79 ± 0.39	0.88	6	12.05

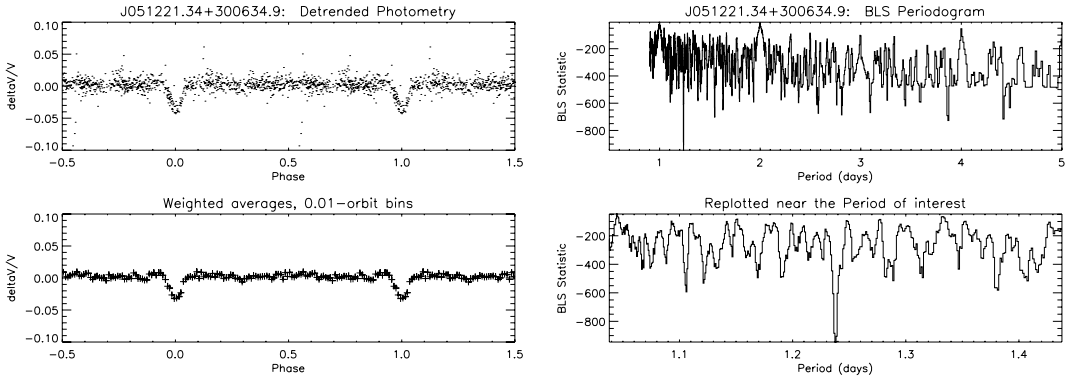

Figure 2. The accepted Priority 1 Candidate J051221.34+300634.9. Left-hand panel: folded light curve. Top panel: folded light curve after detrending. Bottom panel: phase-binned averages weighted by $(1/\sigma_i^2)$, where σ_i^2 is the estimated variance on each data point including both formal and systematic errors (Section 3.1). Right-hand panel: box least-squares periodogram.

and when folded on the most-significant BLS period detection (4.05 d) only shows two transits (we used the next most-significant period of 1.35 d in this analysis). This object is thus kept at Priority 2, pending further light curve sampling in the upcoming 2006 data set.

4.3 Example rejected candidates

(i) *1SWASP J031632.80+300144.2 – ellipsoidal variations.* This object shows six transit-like events of ∼3.1 per cent depth; at this S/N the folded profile (Fig. 4) is not entirely symmetric in the region of the transit, though this may still be an artefact of the reduction. The 2.199-d period is clearly distinct from any aliases in the periodogram, and photometric colours imply a late-G/early-K-type main-sequence parent star. However, the S/N of ellipsoidal variations is high, at ∼26, and indeed a re-plotting of the light curve on a wider phase scale and compressed flux scale shows quite clearly the existence of apparently ellipsoidal variations (compare with e.g. fig. 1 of Sirko & Paczyński 2003). This object is probably a grazing-incidence stellar binary.

(ii) *J040338.43+230237.7 – eccentric-orbit binary?* This object shows pairs of occultations at different depths when folded on the detected period of $1.20 \pm (4.1 \times 10^{-5})$ d, but for which the secondary events are far from phase 0.5 (Fig. 5). The transit-like events are well sampled, with seven transit-like events observed. A further analysis of this interesting object will be reported in a future paper.

(iii) *J044639.17+394837.6 – blend.* This object is apparently very heavily blended and its catalogue magnitudes (e.g. $B \sim 16.5$; no Tycho-2 V magnitude is present for this object) are far from those measured ($V_{\rm SW} \sim 12.0$). The nearby (22 arcsec) object USNO 1298−0108374 has Tycho-2 V magnitude $V_{\rm Ty2} \sim 12.3 \pm 0.4$, much closer to $V_{\rm SW}$. It is surrounded by eight objects within 3.5–5 mag, however, which could contribute up to ∼ 20 per cent of the light in the aperture. Thus, both candidate counterparts are too blended to allow a planetary companion for the observed depth of eclipse-like event.

(iv) *J045349.66+333842.5 – X-ray faint Hα emission-line object.* Rejected because two blended objects are within 5 mag. Simbad shows this to be an Hα emission-line object. No *ROSAT* source is detected. With a 1.8 d period, this might be an X-ray faint active binary with low-amplitude optical variability.

(v) *J040322.73+274841.5 – spectral type uncertainty, blend.* With transit depth of 2 per cent, this object exhibits four transits in the SW-N 2004 data set against otherwise smooth behaviour outside 'transit'. In addition to the candidate, two red objects are found within the aperture that are only 2 mag fainter in $JHK_{\rm s}$ and with USNO magnitude difference from the candidate $\Delta R \sim 5.2$, $\Delta I \sim 3.5$. There is a third neighbour <10 arcsec distant, but it is roughly ∼7 mag fainter (by comparison with a well-separated nearby object of similar apparent brightness in the DSS image). While $(B - V) \sim 0.3$ suggests spectral type roughly ∼F0 or so (Zombeck 1992), $(V_{\rm SW} - K)$ and $(J - H)_{\rm 2MASS}$ suggest spectral type closer to late F or early G. As the SW-N bandpass includes Johnson *RI* (cf. fig. 2 of Kane et al. 2004), this object may well be blended at the 1 per cent level in the SW-N bandpass.

(vi) *J030021.76+275654.3 – artefact.* This object was originally a Priority 2 transit candidate. However, its period and periodogram are highly similar to a number of other distinct stellar objects in the image. The zero-points in the fitted ephemerides for each object are highly similar – with an $\rm MJD_0$ spread of only 1.5 h – suggesting that the apparent period detection may have been dominated by light curve artefacts still present after detrending (Fig. 6). The detrending and BLS period search (Section 3.2) produces a few hundred exoplanet candidates per field, which allows a simple check for candidates that share the same period as several other objects, such as J030021.71+27654.3. In principle, the light curves of all candidates might be examined with reference to the raw image, to determine if such groups of candidates cluster near any bright, variable object or along artefacts such as CCD bleeds. This requires a detailed, highly

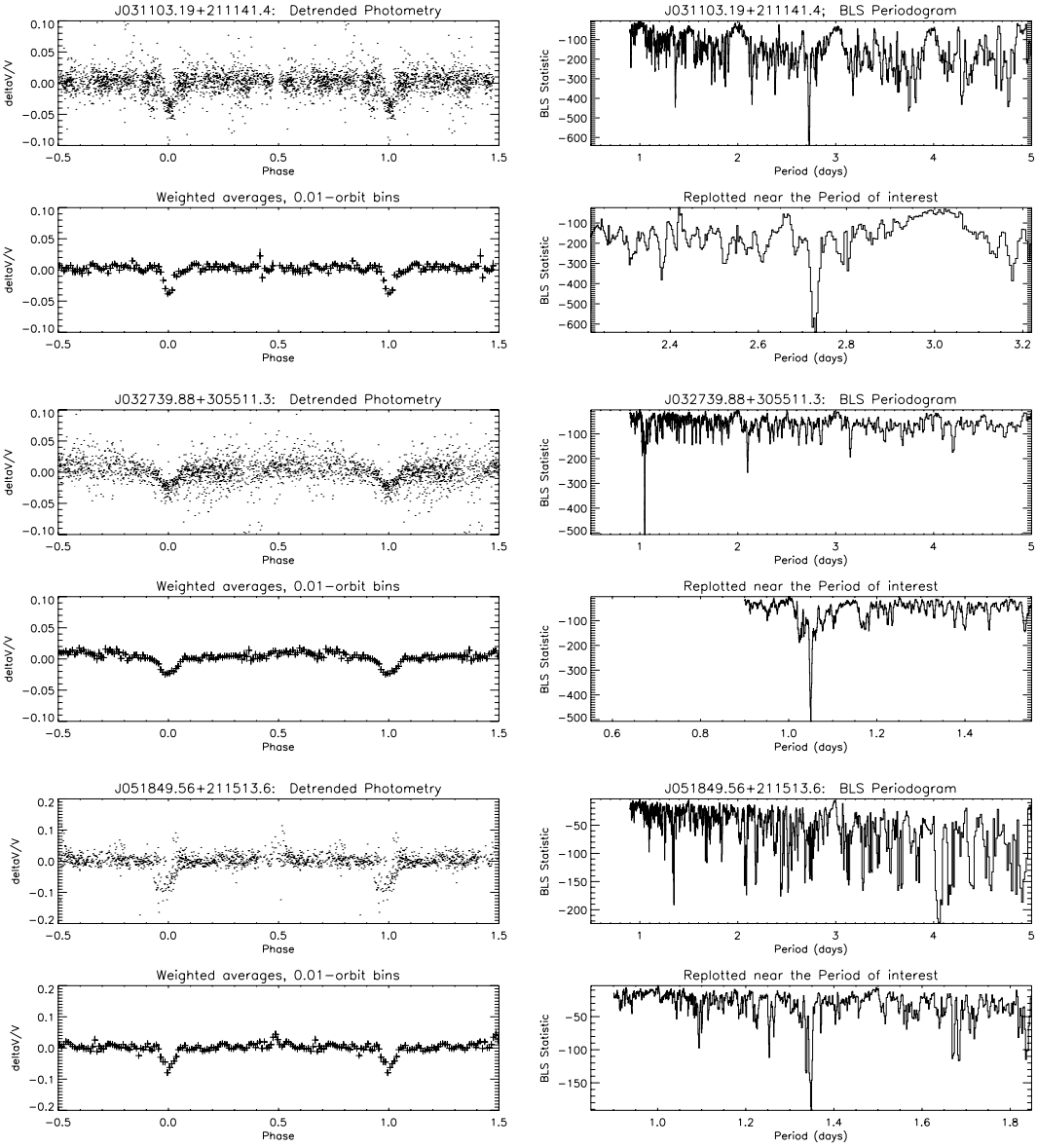

Figure 3. The accepted Priority 2 candidates: folded light curves and BLS periodograms for (from top to bottom panel): J031103.19+211141.4; J032739.88+305511.3 and J051849.56+211513.6.

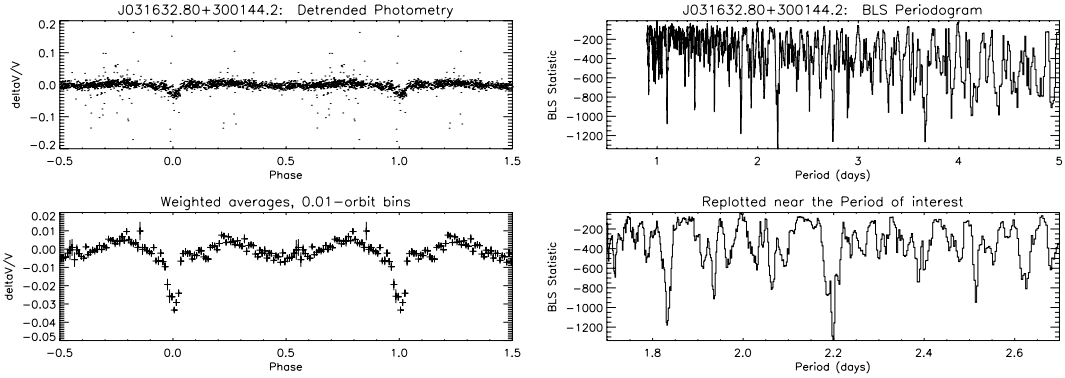

Figure 4. Phase-folded light curve and BLS periodogram of the otherwise excellent transit candidate 1SWASP J031632.80+300144.2. Left-hand panel: the phase-folded light curve as it would appear at the visual examination stage (top) and re-plotted on a compressed flux-scale (bottom); the existence of ellipsoidal variations is clear. (cf. fig. 1 of Sirko & Paczyński 2003.) Right-hand panel: the BLS periodogram.

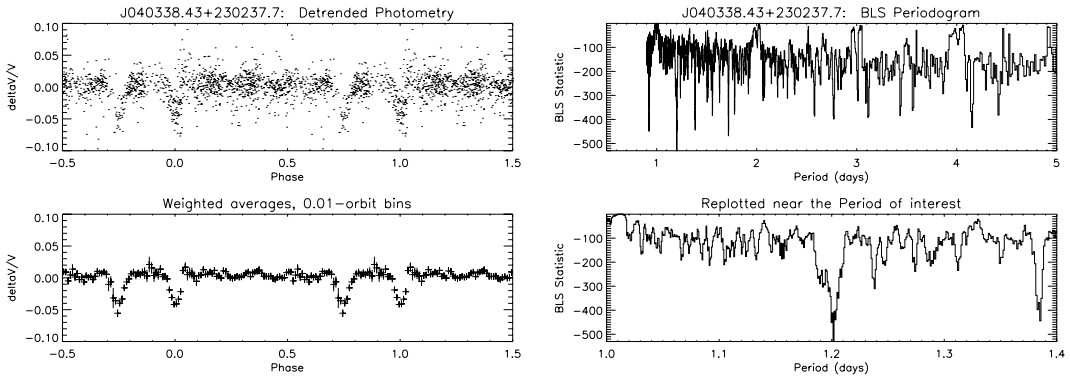

Figure 5. Folded light curve and periodogram for the possible eccentric-orbit system J040338.43+230237.7.

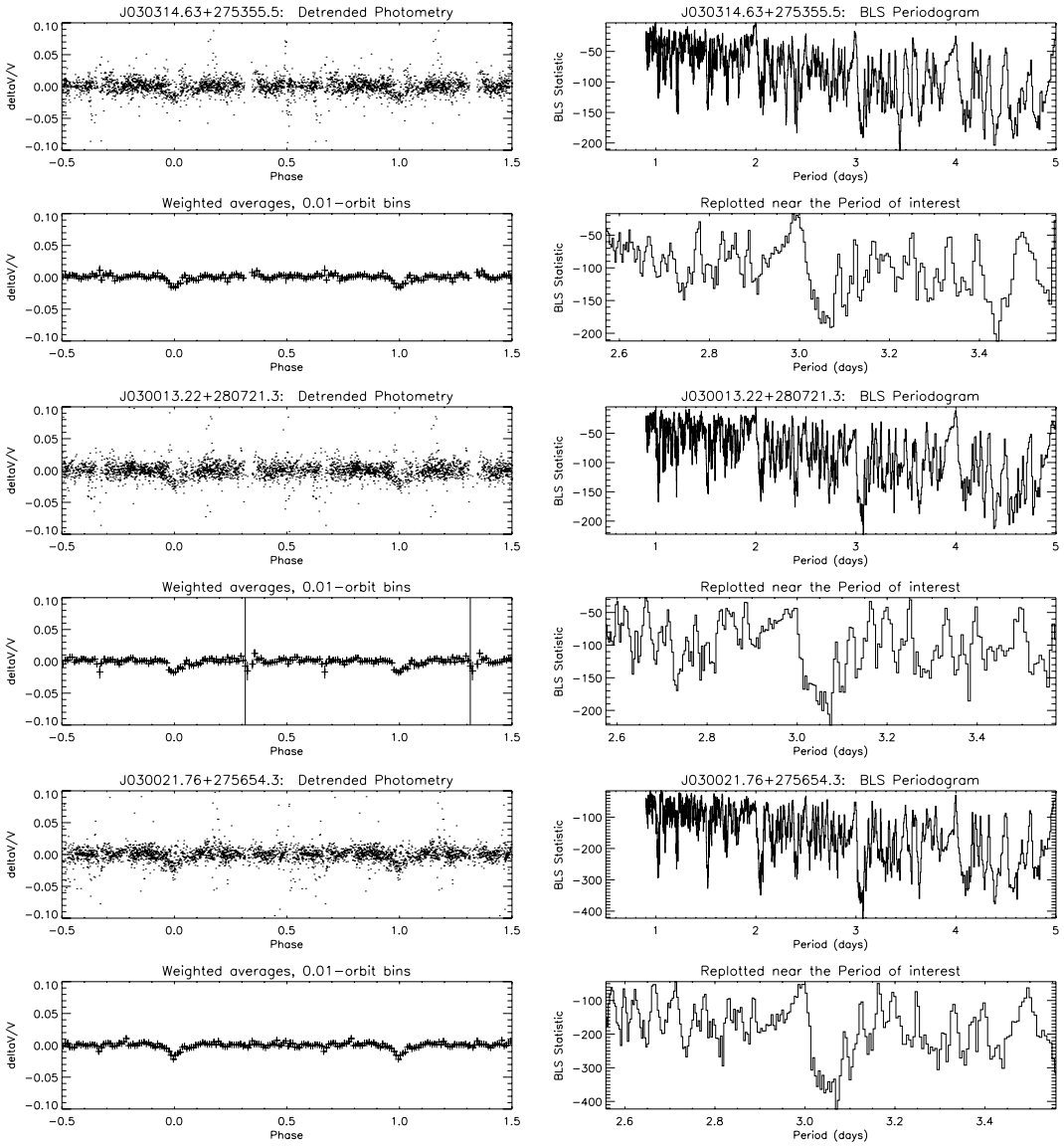

Figure 6. Folded light curves and periodograms (after detrending) for the objects J030314.63+275355.5 (top), J030013.22+280721.3 (middle) and J030021.76+275654.3 (bottom). Detected periods are 3.07125, 3.070201 and 3.0577 d, respectively (from top to bottom). The nearest pair are 10.7 arcmin (43 pixel) from each other but show such similar folded light curves and periods that we reject all three as possible candidates.

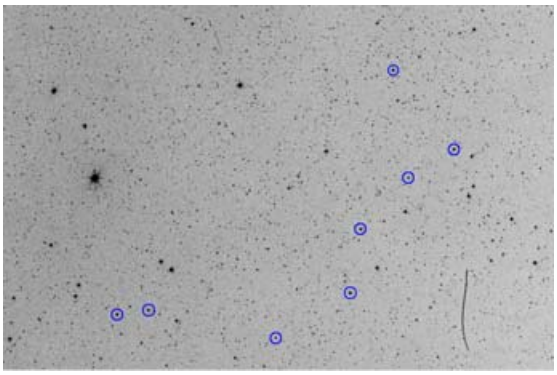

Figure 7. The spatial distribution of objects in field SW3016+3126 with periods 3.06 ± 0.015 d (of which three example light curves are plotted in Fig. 6), overlaid on a Digitized Sky Survey image (the north is at the top and the east is to the left-hand side; the figure measures 90 × 60 arcmin^2 and the objects are marked with the circles). No obvious pattern (such as proximity to a bright source) is seen in the spatial distribution of artefacts. (One further object ∼60 arcmin to the east of this image is not shown).

accurate knowledge of the wings of the point spread function as a function of both on-chip position and frame-number. A simple plot of the position of the candidates with similar periods shows that in fact these objects are *not* near any extremely bright object (Fig. 7).

A more efficient if cruder method is to search for peaks in the distribution of detected periods to catch groups of highly similar detected periods. The distribution of detected periods is highly field-dependent (Fig. 8), so we cannot sum over fields to improve the statistics for this process. We see that for the field containing J030021.76+275654.3 (field SW0316+3126) there is indeed a rather high number (10) of objects with detected period of 3.06 ± 0.015 d. This highlights a number of other suspicious periods from the fields observed. Candidates at these periods were *not* rejected outright based on the period alone, but their light curves and periodograms were compared to other objects with similar detected period to screen for possible artefacts. The sample in Fig. 8 contains light curves both with and without significant sampling gaps – these are the light curves for all objects passed forward for visual selection by the initial BLS period search and statistical cuts (Section 3.2). Objects where the automated search has fit sampling gaps or any residual nightly trends, cluster at 1 d periods; these objects are not considered further. The general shape of the distribution of detected periods does appear to broadly follow the number of nights in each field, though the distribution of periods detected clearly does not depend just on the number of nights alone (Fig. 8). For example, fields SW0344+2427 and SW0543+3126 show similar drops to zero detections at or near periods of integer days, and both are the most sparsely sampled fields in this RA range (Table 1).

(vii) *J032113.37+301909.5 & J032112.56+301910.9 – visual double.* Two separate objects are reported by the WASP pipeline with similar light curves and periodograms, and positions ∼12 arcsec apart. The closeness on-sky of the two light curves threw immediate suspicion on either of these objects as planet-host candidates, which was confirmed at the stage of a catalogue examination. Four catalogues of visual doubles provide matches with this object: the Couteau catalogue of 2700 doubles (Couteau 1995), the Washington Visual Double Star catalogue (Worley & Douglass 1997), the

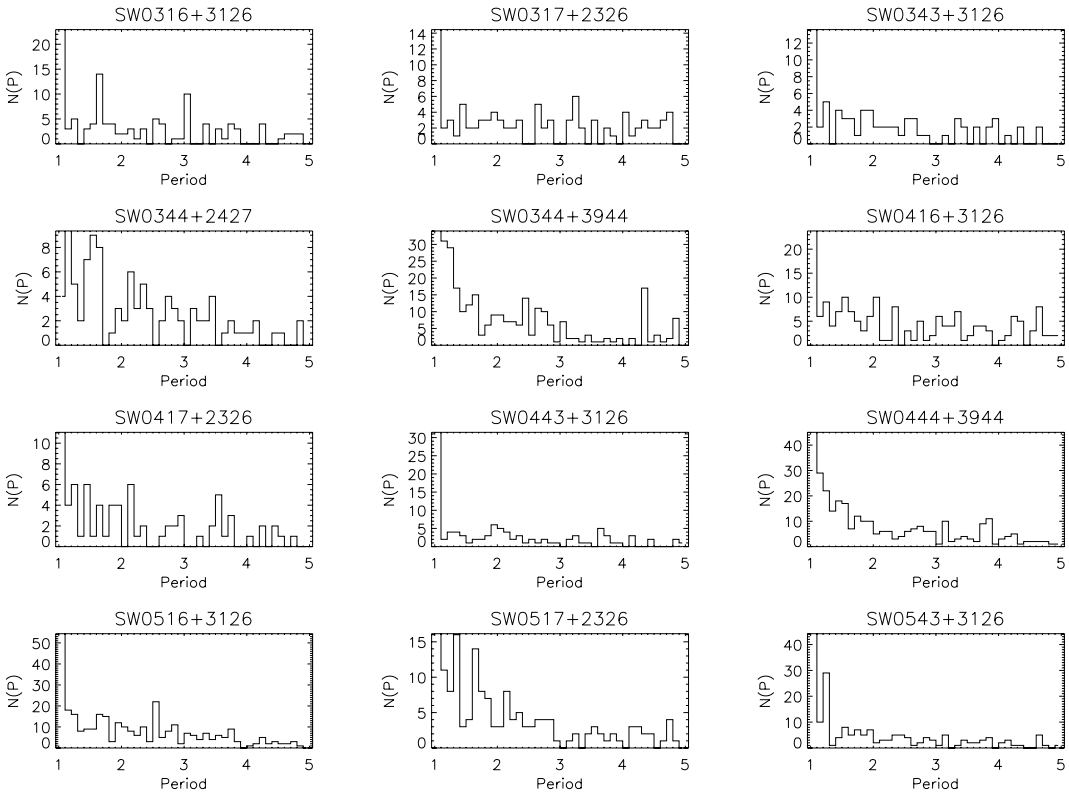

Figure 8. Periodicities returned from BLS period search on light curves that have been detrended (Tamuz et al. 2005). Local increases in the detected period represent possible shared-variability artefacts such as J030021.76+275654.3. The periods at which these likely artefacts occur are highly field-dependent. For example, the field SW0316+3126 (top left-hand panel) shows 10 objects with periods 3.06 ± 0.015 d. An examination of the light curves and periodograms of these objects shows a population of objects with shared variability, which must be removed from further consideration (Fig. 6).

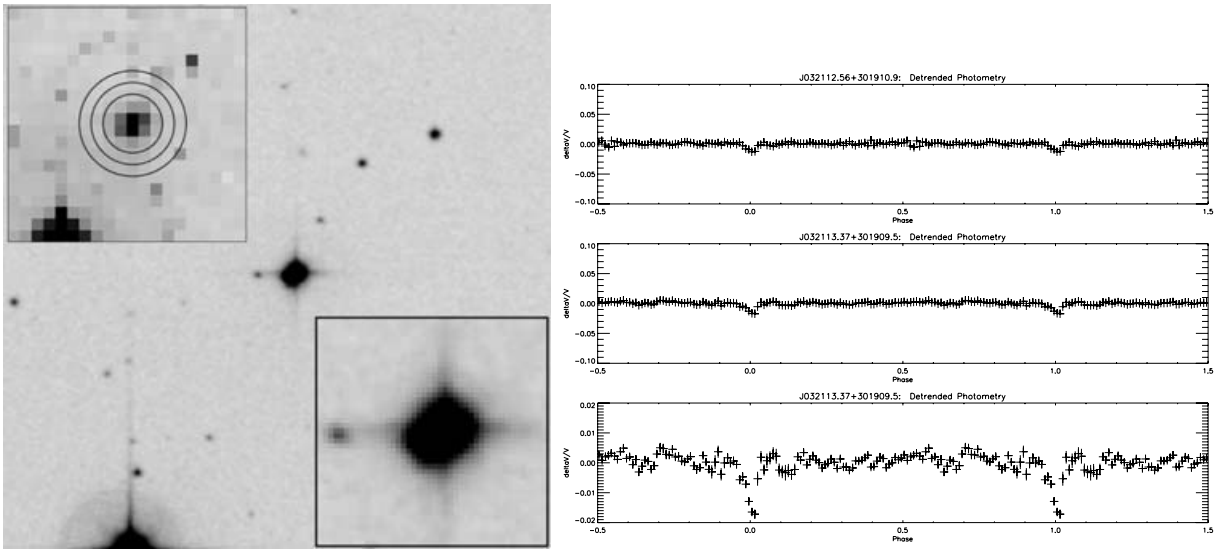

Figure 9. The visual double CCDM J031212+3019A and B, recorded by the WASP pipeline as 1SWASP J032113.37+301909.5 and J032112.56+301910.9 (Section 4.3). Left-hand panel: Digitized Sky Survey image of the 5 × 5-arcmin^2 region surrounding the two objects, with the immediate region surrounding the target (inset lower right-hand side: the inner 30 × 30 arcsec^2) and the full region binned to 15 × 15 arcsec^2 pixels, approximately matching the SW-N pixel scale; Section 2.1 (inset upper left-hand side). The north is up, and the east is to the left-hand side. The three SW-N apertures used for blending tests (2.5, 3.5 and 4.5 pixel) are denoted by concentric circles. At ∼12 arcsec separation, the two components of the visual binary are so close that the resulting source extension under SW-N pixellation in the binned image falls entirely within the innermost aperture; thus the curve-of-growth blending index based on the three SW-N apertures misses the resulting blend. Right-hand panel: light curves of the two objects found by SEXTRACTOR during the pipeline reduction. At 2.27 d, the recurrence interval is rather short for a fully detached stellar binary; however, little indication is found for ellipsoidal variations (bottom right-hand panel).

CCDM (Dommanget & Nys 2002) and the Tycho Double Star Catalogue (Fabricius et al. 2002); this object is the visual double CCDM J03212+3019A and B. The primary is listed as spectral type A5 (luminosity class not determined), and objects A and B have V magnitudes 10.4 and 12.5, respectively. The recurrence interval for the transit-like events is 2.267 42(5) d, which is rather short for a fully detached binary; however, the significance of any ellipsoidal variation is low (at an S/N of ellipsoidal variations $\lesssim$1.7; see also the light curve in Fig. 9). One possible scenario is that the fainter object B may be deeply eclipsed by a third, unseen object. Although only ∼2/3 SW-N pixels apart, the two components do produce an extended object under a 15 arcsec pixel-scale (Fig. 9); initial source finding with SEXTRACTOR (Bertin & Arnouts 1996) localized this to two separate peaks which were each reduced with the WASP pipeline. Although clearly a blend, this object did not fall within the locus of blended objects based on a comparison of flux within the three SW-N apertures, because the object extension falls almost entirely within the innermost aperture (Fig. 9). A further examination of this object will be reported elsewhere.

5 DISCUSSION

Out of a total of 141 895 targets extracted for the transit search in the fields considered here, 2688 were selected as potential photometric transit candidates at the initial selection by $S_{\rm red}$ and cadence by the BLS algorithm (Collier Cameron et al. 2006). Out of these, 44 passed the visual tests. The subsequent statistical tests removed all but 20 of the candidates, of which four passed tests imposed by existing catalogue photometry at higher spatial resolution; this last stage led to the demotion of two otherwise Priority 1 objects. One object was passed forward as a Priority 1 candidate for follow-up with other facilities, with three more flagged as Priority 2 possibilities. As the other WASP candidate lists produced thus far (Christian et al. 2006; Lister et al. 2007; Street et al. 2007) have resulted in approximately three to four times as many good candidates as the fields we report here, it is worth examining the expected planet yield for the RA range 03$^{\rm h}$–06$^{\rm h}$.

The relative dearth of transit candidates reported here is almost certainly a result of the comparatively sparse sampling for this RA range; the most intensively observed field here consisted of 1885 frames over 60 nights, compared to, for example, 5541 frames over 127 nights for a field on the other side of the sky (cf. Street et al. 2007). This has two key effects on our ability to detect transits. The first effect was predicted before the survey began: even with purely uncorrelated noise and an ideal instrument, the rotation of the Earth imposes period ranges in regions about integer-day periods, within which the likelihood of detecting transits is reduced. As the Earth orbits the Sun and the sky precesses throughout the year, the width of these intervals is reduced. These low-observability windows are superimposed on a general decrease in probability of transit observability with period due to fewer numbers of long-period cycles falling within a typical observing season. To clarify this point, we present example estimates of the probability of observing N or more transits in a single SW-N observing season, computed for each field as a byproduct of the transit search (Collier Cameron et al. 2006), with the true sampling of each field as an input (Fig. 10). As can be seen, below about 60 nights' data length, the recoverability of transits drops dramatically for all but the shortest periods.

The second key effect of short observing time-scales is the loss of sensitivity in the presence of strong variability from correlated noise, in which the noise power is not independent of the time-scale of variability. When planning ground-based transit searches, it was largely assumed that improved reduction techniques would result in uncorrelated noise (e.g. Horne 2003). In practice, despite the fact that the magnitude of noise variation from several transit surveys (ours included) approaches the Poisson floor for the entire

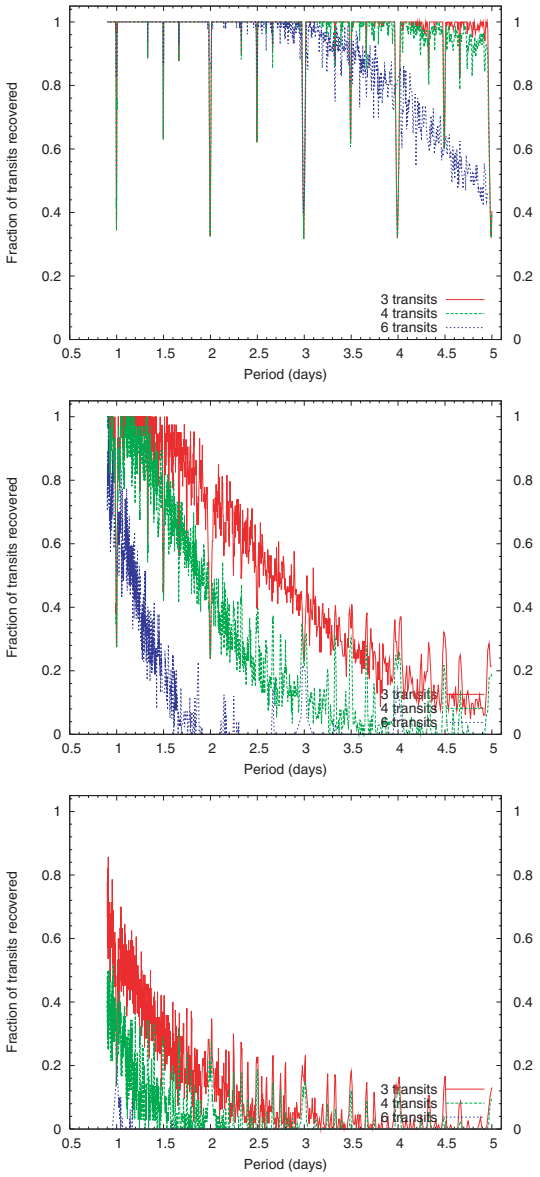

Figure 10. Probability of transit detection as a function of planetary orbital period, for three (solid lines), four (dashed lines) and six (dotted lines) transits (see Collier Cameron et al. 2006). The coverage for these fields is as follows: Top panel: 5441 frames over 129 nights (field 2045+1628); Middle panel: 1402 frames over 64 nights (field SW0343+3126); Bottom panel: 544 frames over 37 nights (SW0543+3126). There is a marked gradient in observability of transits with the number of nights observed; for 37 nights of data, the recovery fraction at four transits drops to 10 percent at all periods $\gtrsim$1.5 d.

magnitude range over which we are sensitive to transits (here $8 \lesssim V \lesssim 13$), correlated noise continues to be a significant source of potential false-positives, with significant power to variations with $\sim$2.5 h duration (similar to a genuine exoplanet transit). The only ground-based broad-shallow transit-search team we are currently aware of the claims that uncorrelated noise is the XO group, which employs drift-scanning to smooth out systematic trends instrumentally (McCullough et al. 2006); thus it appears that correlated noise of this nature may be a feature of the observational strategy we have chosen. The full S/N statistic $S_{\rm red}$ of Pont et al. (2006) provides a measure of the S/N of a transit detection in the presence of correlated noise, and thus provides a useful measurement to investigate ways to tame frequency-dependent correlated noise. In particular, we note the following two key results from the considerations of Pont et al. (2006): (i) that for ground-based transit surveys the threshold to detect transits in the presence of correlated noise is typically a factor $\sim$3 higher than in the presence of uncorrelated noise alone, and that (ii) in the presence of correlated noise, $S_{\rm red}$ should scale roughly linearly with the total number of nights of observation. The latter is particularly important, and can be easily understood in the following way: consider a transit signal with transit duration $\delta_{\rm t}$ and period $P_{\rm t}$. The presence of correlated noise with significant power at time-scales $\sim \delta_{\rm t}$ will add spurious transit-like events at randomized phases, reducing the coherence of the resulting transit light curve and making the true periodicity more difficult to separate out from the noise. Although a comparison of the badness-of-fit allowing a model consisting of both positive and negative transit-like events with that from negative transits only (cf. Burke et al. 2006) can to some extent estimate the impact of correlated noise on the light curve itself; it is clear that characterization of the true transit period in this case really requires as long an observing season as possible.

Indeed, simulations applied specifically to the WASP project (Smith et al. 2006) suggest that $S_{\rm red}$ should increase roughly linearly with the number of nights of observation; Smith et al (2006) suggest that $\sim 19 \pm 8$ genuine detections should be expected from the entire WASP-N 2004 data set; at $\lesssim$60 nights the recovery fraction drops to roughly a quarter of that expected for data sets of length $\sim$120 nights. Our yield of four candidates is consistent with this scaling.

6 CONCLUSIONS

One Priority 1 exoplanet transit candidate has been uncovered from fields with RA $03^{\rm h}$–$06^{\rm h}$ in the WASP-N 2004 data set and three Priority 2 objects. This number is lower than that produced by other fields with longer observation time bases. This is certainly due to the comparatively sparse sampling, which bears out in a qualitative way the results of recent work on correlated noise in ground-based photometric surveys. When the 2006 SuperWASP data sets are fully reduced, we expect to find many more candidates for follow-up work as a result of the longer baseline this allows.

ACKNOWLEDGMENTS

The WASP consortium consists of representatives from the Queen's University Belfast, University of Cambridge (Wide Field Astronomy Unit), Instituto de Astrofisica de Canarias, Isaac Newton Group of Telescopes (La Palma), University of Keele, University of Leicester, Open University, and the University of St Andrews. The SuperWASP-North and South instruments were constructed and operated with funds made available from Consortium Universities and the Particle Physics and Astronomy Research Council. SuperWASP I is located in the Spanish Roque de Los Muchachos Observatory on La Palma, Canary Islands which is operated by the Instituto de Astrofsica de Canarias (IAC). Several large astronomical catalogues were used via the VIZIER service, operated at CDS in Strasbourg, France, primarily the Tycho-2 and USNO catalogues. This publication makes use of data products from 2MASS, which is a joint project of the University of Massachusetts and the Infrared Processing and Analysis Centre/California Institute of Technology, funded by the National Aeronautics and Space Administration and the National Science Foundation. The Digitized Sky Surveys were produced at the Space Telescope Science Institute under US Government grant NAG W-2166. The images of these surveys are based

on photographic data obtained using the Oschin Schmidt Telescope on Palomar Mountain and the UK Schmidt Telescope. The plates were processed into the present compressed digital form with the permission of these institutions. We have made use of the Extrasolar Planets Encyclopaedia, maintained online by Jean Schneider at http://exoplanet.eu/catalog.php.

We thank the anonymous referee for a number of insightful comments that greatly improved this manuscript. WIC thanks Peter McCullough and Kailash Sahu for fruitful discussion.

REFERENCES

Aigrain S., Favata F., 2002, A&A, 395, 625
Aigrain S., Irwin J., 2004, MNRAS, 350, 331
Ammons S. M., Robinson S. E., Strader J., Laughlin G., Fischer D., Wolf A., 2006, ApJ, 638, 1004
Bakos G. et al., 2007a, ApJ, 656, 552
Bakos G. A. et al., 2007b, ApJ, submitted, (arXiv:0705.0126)
Bertin E., Arnouts S., 1996, A&AS 117, 393
Bessell M. S., Brett J. M., 1988, PASP 100, 1134
Binney J. J., Merrifield M., 1998, Galactic Astronomy, 1st edn. Princeton Univ. Press, Princeton, NJ
Blackwell D. E., Lynas-Gray A. E., 1998a, VizieR On-line Data Catalog: J/A+AS/129/505
Blackwell D. E., Lynas-Gray A. E., 1998b, A&AS, 129, 505
Bouchy F., Pont F., Melo C., Santos N. C., Mayor M., Queloz D., Udry S., 2005, A&A, 431, 1105
Brown T. M., 2003, ApJ, 593, L125
Brown T. M., Charbonneau D., Gilliland R. L., Noyes R. W., Burrows A., 2001, ApJ, 552, 699
Burke C. J., Gaudi B. S., DePoy D. L., Pogge R. W., 2006, AJ 132, 210
Burke C. J. et al., 2007, ApJ, submitted, (arXiv:0705.0003)
Carpenter J. H., 2001, AJ, 121, 2581
Carter B. S., 1990, MNRAS, 242, 1
Cayrel de Strobel G., Soubiran C., Ralite N., 2001, A&A, 373, 159
Charbonneau D., Brown T. M., Noyes R. W., Gilliland R. L., 2002, ApJ, 568, 377
Charbonneau D. et al., 2006, ApJ, 636, 445
Charbonneau D., Brown T. M., Burrows A., Laughlin G., 2007a, in Reipurth V. B., Jewitt D., Keil K., eds, Protostars and Planets V. University of Arizona Press, Tucson, p. 701
Charbonneau D., Winn J. N., Everett M. E., Latham D. W., Holman M. J., Esquerdo G. A., O'Donovan F. T., 2007b, ApJ, 658, 1322
Christian D. J. et al., 2006, MNRAS, 372, 1117
Collier Cameron A. et al., 2006, MNRAS, 373, 799
Collier Cameron A. et al., 2007, MNRAS, 375, 951
Couteau P., 1995, VizieR On-line Data Catalog: I/209A
Deming D., Seager S., Richardson L. J., Harrington J., 2005a, Nat, 434, 740
Deming D., Brown T. M., Charbonneau D., Harrington J., Richardson L. J., 2005b, ApJ, 622, 1149
Dommanget J., Nys O., 2002, VizieR On-line Data Catalog: I/274
Fabricius C., Høg E., Makarov V. V., Mason B. D., Wycoff G. L., Urban S. E., 2002, A&A, 384, 180
Foqué P., Gieren W. P., 1997, A&A, 320, 799
Fruscione A., Hawkins I., Jelinsky P., Wiercigroch A., 1994, ApJS 94, 127
Glass I. S., 1999, Handbook of Infrared Astronomy, 1st edn. Cambridge Univ. Press, Cambridge
Gould A., Morgan C. W., 2003, ApJ, 585, 1056
Gray D. F., 1992, The Observation and analysis of stellar photospheres, 2nd edn. Cambridge Univ. Press, Cambridge
Høg E. et al., 2000, A&A, 355, 27
Homer L., Charles P. A., Hakala P., Muhli P., Shih I.-C., Smale A. P., Ramsay G., 2001, MNRAS, 322, 827
Horne K., 2003, in Deming D., Seager S., eds, ASP Conf. Ser. Vol. 294, Scientific Frontiers in Research on Extrasolar Planets. Astron. Soc. Pac., San Francisco, p. 361
Kane S. R., Collier Cameron A., Horne K., James D., Lister T. A., Pollacco D. L., Street R. A., Tsapras Y., 2004, MNRAS, 353, 689
Kervella P., Thévenin F., Di Folco E., Ségransan D., 2004, A&A, 426, 297
Kovács G., Zucker S., Mazeh T., 2002, A&A, 391, 369
Lister T. A. et al., 2007, MNRAS, 379, 647
Mayor M., Queloz D., 1995, Nat, 378, 355
McCullough P. R. et al., 2006, ApJ, 648, 1228
Monet D. G. et al., 2003, AJ, 125, 984
Moutou C. et al., 2006, A&A, 458, 327
Nikolaev S., Weinberg M. D., Skrutskie M. F., Cutri R. M., Wheelock S. L., Gizis J. E., Howard E. M., 2000, AJ, 120, 3340
Pollacco D. L. et al., 2006, PASP, 118, 1407
Pollack J. B., Hubickyj O., Bodenheimer P., Lissauer J. J., Podolak M., Greenzweig Y., 1996, Icarus, 124, 62
Pont F., Zucker S., Queloz D., 2006, MNRAS, 373, 231
Richardson L. J., Deming D., Seager S., 2003, ApJ, 597, 581
Sahu K. C. et al., 2006, Nat 443, 534
Sirko E., Paczyński B., 2003, ApJ, 592, 1217
Smith A. M. S. et al., 2006, MNRAS, 373, 1151
Stetson P. B., 1990, PASP 102, 932
Street R. A. et al., 2003, MNRAS, 340, 1287
Street R. A. et al., 2007, MNRAS, 379, 816
Tamuz O., Mazeh T., Zucker S., 2005, MNRAS, 356, 1466
Tingley B., Sackett P. D., 2005, ApJ, 627, 1011
Torres G. et al., 2007, ApJ, in press, (arXiv:0707.4268)
Udalski A., Paczynski B., Zebrun K., Szymanski M., Kubiak M., Soszynski I., Szewczyk O., 2002a, Acta Astron., 52, 1
Udalski A., Zebrun K., Szymanski M., Kubiak M., Soszynski I., Szewczyk O., Wyrzykowski L., Pietrzynski G., 2002b, Acta Astron., 52, 115
Udalski A., Szewczyk O., Zebrun K., Pietrzynski G., Szymanski M., Kubiak M., Soszynski I., Wyrzykowski L., 2002c, Acta Astron., 52, 317
Udry S. et al., 2000, A&A, 356, 590
Valenti J. A., Fisher D. A., 2005, ApJS 159, 141
Vidal-Madjar A. et al., 2004, ApJ, 604, L69
Wilson D. M. et al., 2007, in Alfonso C., Weldrake D., Henning T. H., eds, ASP Conf. Vol. 118, Transiting Extrasolar Planets Workshop, Astron. Soc. Pac., San Francisco, p. 187
Worley C. E., Douglass G. G., 1997, A&AS, 125, 523
Zombeck M. V., 1992, Handbook of Space Astronomy and Astrophysics, 2nd edn. Cambridge Univ. Press, Cambridge

This paper has been typeset from a TEX/LATEX file prepared by the author.